Development of a novel boring tool with anisotropic dynamic stiffness to avoid chatter vibration in cutting

Part 1: Design of anisotropic structure to attain infinite dynamic stiffness

Wataru Takahashi[1], Norikazu Suzuki[2], Eiji Shamoto[2]

Affiliations: [1] Mitsubishi Materials Corpration, 1-600 Kitabukuro-cho, Omiya-ku, Saitama-Shi, Saitama, 330-8508, Japan

[2] Nagoya University, Furo-cho, Chikusa-ku, Nagoya, 464-8603, Japan

This paper presents a novel design method of the anisotropic structure to attain infinite dynamic stiffness to avoid chatter vibration in boring operations. Because a long and slender tool is used for boring operations, the stiffness of the tool holder is likely to decrease, resulting in low chatter stability. Although it is difficult to improve the stiffness of the boring holder itself, the nominal dynamic stiffness for the cutting process can be improved by designing an appropriate anisotropy in the dynamic stiffness of the boring tool. In this study, we formulate a theoretical relationship between the mechanical structural dynamics and chatter stability in boring operation and present the basic concept of tool design with anisotropic structure. In the actual tool design, ideal anisotropy may not be realized because of the influence of design error. Therefore, an analytical study was conducted to clarify the influence of the design error on the vibration suppression effect. Analytical investigations verified that the similarity of the frequency response functions in the modal coordinate system and the design of the compliance ratio according to the machining conditions are important. Furthermore, we designed a boring tool with an anisotropic structure which can achieve the proposed anisotropic dynamics. The frequency response function was evaluated utilizing FEM analysis. The estimated anisotropic dynamics of the proposed structure could significantly improve the nominal dynamics for boring operations.

Key words: Cutting, Chatter, Boring, Dynamic stiffness, Anisotropy, Stability

1. Introduction

Cutting operations are widely used in the process of manufacturing of products that require flexibility with respect to the machinable shape and machining quality. Cutting operations are particularly indispensable in boring operations, which are widely employed in mechanical construction. Boring operations with boring tools can set up arbitrary hole diameters regardless of the tool diameter. It can simultaneously achieve highly accurate processing and is thus often used in production sites. However, boring operations require thinly protruding tools with a diameter smaller than the machining hole, resulting in problematic tendencies such as decreasing stiffness of the tool holder and the onset of chatter vibration. The machining efficiency and product quality both directly influence production costs; thus, avoiding chatter vibration is one of the most important issues in cutting operations. The mechanism of chatter vibration is known to be caused by mutual interactions between the dynamic behavior of the mechanical structure and the machining process accompanying regenerative effects. Furthermore, chatter vibration is likely to occur when the structural stiffness of the operating system is low (e.g., during boring operations); once chatter vibration has appeared, it can deteriorate the finished surface as well as damage the tools, workpieces, and machine tools. Therefore, many researchers have focused on analysis and suppression techniques of chatter vibration [1].

Increasing the stiffness of the machine structure is generally necessary for suppressing chatter vibration. Supports (e.g., jigs) are effective in improving the stiffness of a mechanical structure [2]. Meanwhile, supports cannot be easily used in boring operations because of the constraints in the machining shape. Therefore, an approach that focuses on the material of the tool holder is often used in boring operations. Steel is generally used as the material for the tool holder; however, sintered tungsten carbide which has a higher stiffness is used when measures against chatter vibration must be taken. Furthermore, techniques to change a portion of the tool holder material have been proposed. For example, Thorenz et al. proposed a technique which used a carbon fiber reinforced plastic (CFRP) for a part of the tool holder material [3]. This reduced the mechanical compliance of the structure by inserting a CFRP core in the internal area of the tool holder and increasing its damping performance. Furthermore, Yuhuan et al. proposed a CFRP boring tool that used constrained layer damping (CLD) to further improve the damping performance of the composite boring tool [4]. Ghorbani et al. employed epoxy granite which has higher damping characteristics than steel as the tool holder material [5]. Denkena et al. proposed an anti-vibration

technique that incorporated friction dampers inside a tool holder [6]. Furthermore, Paul et al. proposed a technique in which metallic particles were sealed within the tool holder and which used the impact attenuation of the weights attached to the sides [7]. All these methods suppressed the chatter vibration and improved the processing surface roughness. However, the disadvantage of these methods is the higher cost of these materials than that of steel.

Methods that use tuned mass dampers (TMDs) have been proposed by many researchers as a different effective approach because there are limits to the improvements that can be made in a tool holder material. The suitable use of this method can greatly reduce compliance at the natural frequency. However, tool holders used in boring operations can cause interference with the workpiece when the TMD structure is attached to the external section of the tool; thus, a mass damper needs to be fabricated into the tool holder. Onozuka et al. proposed a setup that maximized the built-in TMD performance while controlling the reduction in structural stiffness using structural analysis [8]. Slocum et al. proposed a built-in TMD technique which used a viscous fluid as a damper to improve the robustness against vibration frequency and amplitude [9]. Numerous other proposed anti-vibration techniques that modify the holder have been proposed [10-14]. However, reducing the diameter is difficult for application of TMD because of the complex shank structure of the tool, in addition to the cost issues. Therefore, the practical application of many of these methods is difficult.

Another proposed method involved avoiding chatter by actively using sensors or actuators. Matsubara et al. incorporated a sensor and a piezoelectric actuator in a boring tool and proposed a technique that the reduced nominal compliance by creating an inductor-resistor (LR) circuit that functioned as a mechanical vibration device [15]. Chen et al. proposed a static/dynamic stiffness improvement technique which used a linear magnetic actuator with three degrees of freedom and achieved improved stability with respect to the chatter vibration in boring operations [16]. Furthermore, Wang et al. proposed a boring tool structure that incorporated an electrorheological fluid within the structure. This improved the dynamic characteristics of the boring tool by detecting the chatter vibration using the sensor and controlling the electrorheological fluid according to the detected signal [17]. In addition, techniques that avoid chatter vibration using feed drive control of the machine tool without using any additional actuators have been proposed. Among these, Fallah et al. proposed using a filtered-x normalized least mean square method that included feedback control [18], as well as chatter vibration control techniques that extended the

control setup of the feed drive system in a CNC machine tool. Limited effects can be expected from each of these methods; however, these are not universally effective and decisive methods.

Suzuki et al. clarified that anisotropy of the mechanical structure considerably influenced the stability of chatter vibration [19]. This charateristics was used, and the desired anisotropy was intentionally designed in the tool holder to propose a method that made the nominal dynamic stiffness of the chatter vibration infinitely large relative to the changes in the cutting force, and the basic principle governing this method was explained [20]. This method could improve the nominal stiffness by designing a simple desired shape in the tool shank and applying anisotropy to it. In other words, chatter vibration in boring operations can be avoided without involving complex or high-cost structures used in conventional techniques. Takahashi et al. used these ideas and designed a tool shank shape with a conventionally impossibly large L/D [21]. However, no quantitative analyses of these vibration control effects were conducted, and the influence of the design errors during tool setup on the vibration suppression effects was also not clarified. Furthermore, the proposed methods were not experimentally verified. In other words, the feasibility of this proposed method has not yet been demonstrated. Thus, the present study seeks to clarify the feasibility of techniques that infinitely increase the stiffness using the anisotropy of the mechanical structure. Part 1 analyzes the characteristics of the proposed technique primarily through analytical methods and predicts the expected improvements in the nominal dynamic stiffness effects. Part 2 analyzes the stability limit of the prototyped tools and clarifies the issues related to the potential of employing the proposed method using primarily experimental methods and issues related to practical applications.

Section 2 of this manuscript (Part 1) will discuss the chatter vibration mechanisms and process models of the boring operation. In Section 3, the theory of infinitely large stiffness due to anisotropy design in the mechanical structure is discussed, which Section 4 details the proposed tool design method using the finite element method (FEM) and provides examples. Conclusions are presented at the end of the paper.

2. Analysis model of chatter vibration stability limit during boring

This section explains the modeling of the boring process and the stability limit analysis methods for chatter vibration. A schematic diagram of the boring process is shown in Fig. 1. Inside the hole surface, operations are conducted by attaching an insert tool to the elongated tool holder and applying a feed

motion parallel to the rotational axis. In this study, the workpiece was presumed to rotate around the z-axis, and a feed motion was applied in the z-axis direction relative to the tool. The tool was elongated, and its axis was parallel to the z-axis. The stiffness was likely to decrease in the directions of the radial x- and y-axes; thus, it was assumed that the tool could vibrate in the direction of the x,y plane, and other mechanical structures could not vibrate. Furthermore, the vibration in the cutting direction (y-axis direction) intrinsically had no influence on the changes in chip thickness; the influences due to this cutting process were ignored. As shown in the enlarged section of the cutting section, d_r is the radial depth of cut, and c is the feed rate for spindle rotation. The projection width of the cutting edge range contacting the workpiece along the z-axis direction was set as the cutting width b. Of this cutting range, the projection component of the contact width between the cutting edge and workpiece prior to a single rotation was set as the regenerative width b_d. These widths are nominal dimensions that ignore the influence of tool vibration and can be calculated from the cutting conditions and tool shape alone.

The relative tool–workpiece displacement in the x-axis direction at time t is set as $u_x(t)$. If a single period of the spindle revolution is set as T, the relative displacement prior to the single period is given by $u_x(t-T)$. The amount of variation of the cutting cross-sectional area at time t is set as $\Delta s(t)$ and is given by Eq. (1).

$$\Delta s(t) = b u_x(t) - b_d u_x(t-T) \qquad (1)$$

Furthermore, chips are thought to follow Colwell's model [22] and flow in the vertical direction at an angle diagonal to the cutting cross-section. The cutting force is assumed to be mainly generated in the chip flow direction and cutting direction. Here, we consider an orthogonal cutting direction defined by the cutting direction and chip flow direction. However, the oblique angle of the tool is ignored. The specific cutting force components of the principal force and the thrust force directions for orthogonal cutting are K_p and K_t, respectively, and the specific cutting force in the radial cutting direction (x direction) is set as $K_f = K_t \cos\eta$. Here, η is the chip flow angle. Among the cutting forces in the x and y directions at time t, the force fluctuation component $\Delta \boldsymbol{F}$ caused by vibration displacement is given by Eq. (2).

$$\Delta \boldsymbol{F}(t) = \begin{Bmatrix} \Delta F_x(t) \\ \Delta F_y(t) \end{Bmatrix} = \begin{Bmatrix} -K_t \cos\eta \, \Delta s(t) \\ -K_p \Delta s(t) \end{Bmatrix} \qquad (2)$$

$$= \begin{Bmatrix} 1 \\ 1/K_r \cos\eta \end{Bmatrix} \Delta F_x(t)$$

$K_r \left(= K_t/K_p\right)$ is the force ratio. Here, the effects of the edge force are ignored. Eq. (1) is substituted to obtain Eq. (3).

$$\begin{aligned} \Delta \boldsymbol{F}(t) &= \begin{Bmatrix} \Delta F_x(t) \\ \Delta F_y(t) \end{Bmatrix} \\ &= -K_t \cos\eta \begin{Bmatrix} 1 \\ 1/K_r \cos\eta \end{Bmatrix} \left(b u_x(t) b_d u_x(t-T) \right) \end{aligned} \tag{3}$$

The two-degree-of-freedom system transfer function of the boring tool is set as $\boldsymbol{G}(s)$. The vibration displacement $\boldsymbol{u}(i\omega_c)$ at an angular frequency of chatter vibration ω_c is expressed using Eq. (4).

$$\begin{aligned} \boldsymbol{u}(i\omega_c) &= \begin{Bmatrix} u_x(i\omega_c) \\ u_y(i\omega_c) \end{Bmatrix} = \\ & \begin{bmatrix} G_{xx}(i\omega_c) & G_{xy}(i\omega_c) \\ G_{yx}(i\omega_c) & G_{yy}(i\omega_c) \end{bmatrix} \begin{Bmatrix} \Delta F_x(i\omega_c) \\ \Delta F_y(i\omega_c) \end{Bmatrix} \end{aligned} \tag{4}$$

From Eq. (2), the vibration displacement $u_x(i\omega_c)$ in the cutting direction for the frequency domain can be expressed by Eq. (5) using the force fluctuation amount $\Delta F_x(i\omega_c)$ in the cutting direction.

$$\begin{aligned} u_x(i\omega_c) &= G_{xx}(i\omega_c)\Delta F_x(i\omega_c) \\ &\quad + G_{xy}(i\omega_c)\Delta F_y(i\omega_c) = \\ &\left(G_{xx}(i\omega_c) + \frac{G_{xy}(i\omega_c)}{K_r \cos\eta} \right) \Delta F_x(i\omega_c) \end{aligned} \tag{5}$$

This is the nominal equation of motion in the direction of the x-axis, which relates the variations in the cutting force and the structural displacement in the radial depth of cut direction during the turning process. Thus, the vibration displacement $u_x(i\omega_c)$ in the radial depth of cut direction for the frequency domain can be expressed with one degree of freedom. This frequency response function with one degree of freedom can be expressed as $\Phi_0(i\omega_c)$ using the following equation:

$$\Phi_0(i\omega_c) = G_{xx}(i\omega_c) + \frac{G_{xy}(i\omega_c)}{K_r \cos\eta} \tag{6}$$

In other words, the dynamic characteristics of the cutting system are not only influenced by the diagonal component G_{xx} of the transfer function but also by the off-diagonal element G_{xy}. This influence depends

on the cutting force ratio K_r and the chip flow angle η. Eq. (7) and (8) are then obtained by substituting Eq. (5) and (6) into Eq. (3).

$$\Delta F_x(i\omega_c) = -K_t(b_d + c - b_d e^{-i\omega_c T}) \Phi(i\omega_c)\Delta F_x(i\omega_c) \tag{7}$$

$$\begin{aligned}\Phi(i\omega_c) &= \cos\eta\, \Phi_0(i\omega_c) \\ &= \cos\eta\, G_{xx}(i\omega_c) + \frac{G_{xy}(i\omega_c)}{K_r}\end{aligned} \tag{8}$$

The value of $\Phi(i\omega_c)$ in Eq. (8) is the one-degree-of-freedom frequency response function, which considers the effects of the chip flow direction and force ratio in the turning process, and the present study defines this as the equivalent transfer function. The following equation needs to be satisfied for Eq. (7) to hold when $\Delta F_x(i\omega_c)$ is a non-zero value.

$$1 + K_t(b_d + c - b_d e^{-i\omega_c T})\Phi(i\omega_c) = 0 \tag{9}$$

The stability limit of the system can be obtained by solving for this characteristic equation in the cutting process. Note that $\Phi(= \cos\eta\, \Phi_0)$ is the nominal dynamic stiffness that represents the system and is an important indicator for stability assessment. A block diagram of the formulated process is shown in Fig. 2.

3. Theory of anisotropy design for infinitely large stiffness

This section explains the fundamental design principles of anisotropic transfer characteristics to achieve an infinitely large stiffness. Afterwards, the influence of parameter error is analytically investigated. First, as shown in Eq. (8), the dynamic characteristics of the cutting process are influenced not only by the diagonal component of the transfer function but also by the off-diagonal component, force ratio, and chip flow angle. In contrast, this suggests that appropriate design of the off-diagonal component of the transfer function and force ratio as well as the chip flow angle can reduce the nominal compliance. Thus, it is technically difficult to simply increase the stiffness of the diagonal component of the transfer function; however, that offsetting this influence using anisotropy could achieve increased stiffness. This should improve the stability limit of chatter vibration. Suzuki et al. proposed a method to design an arbitrary

anisotropy by shifting the mode ratio of the two-degree-of-freedom system from one and furthermore rotating the coordinate system [19]. Here, the following equation considers the vibration system in each direction for an orthogonal pq coordinate system (modal coordinate system).

$$
{}^{pq}\boldsymbol{G}(s) = \begin{bmatrix} G_{pp}(s) & G_{pq}(s) \\ G_{qp}(s) & G_{qq}(s) \end{bmatrix}
$$

$$
= \begin{bmatrix} \dfrac{\omega_{np}^2/k_p}{s^2 + 2\zeta_p\omega_{np}s + \omega_{np}^2} & 0 \\ 0 & \dfrac{\omega_{nq}^2/k_q}{s^2 + 2\zeta_q\omega_{nq}s + \omega_{nq}^2} \end{bmatrix} \quad (10)
$$

where ω_n, ζ, and k are the modal parameters in each direction and represent the natural frequency, damping ratio, and spring stiffness. ω_n and ζ are equivalent in each direction (i.e., $\omega_{np} = \omega_{nq}, \zeta_p = \zeta_q$), whereas k changes for each direction ($k_p \neq k_q$). As shown in Fig. 3, the transfer function ${}^{xy}\boldsymbol{G}(s)$ in the xy coordinate system, where the pq coordinate system is rotated by θ (process coordinate system), is obtained using Eq. (11).

$$
{}^{xy}\boldsymbol{G}(s) = \begin{bmatrix} G_{xx} & G_{xy} \\ G_{yx} & G_{yy} \end{bmatrix} =
$$

$$
\begin{bmatrix} \cos\theta & -\sin\theta \\ \sin\theta & \cos\theta \end{bmatrix}^{-1} \begin{bmatrix} G_{pp} & G_{pq} \\ G_{qp} & G_{qq} \end{bmatrix} \begin{bmatrix} \cos\theta & -\sin\theta \\ \sin\theta & \cos\theta \end{bmatrix} \quad (11)
$$

Here, the off-diagonal component of the transfer function ${}^{pq}\boldsymbol{G}(s)$ in the pq coordinate system is zero, which provides Eq. (12).

$$
\begin{bmatrix} G_{xx} & G_{xy} \\ G_{yx} & G_{yy} \end{bmatrix} =
$$

$$
\begin{bmatrix} \cos^2\theta\, G_{pp} + \sin^2\theta\, G_{qq} & -\sin\theta\cos\theta\,(G_{pp} - G_{qq}) \\ -\sin\theta\cos\theta\,(G_{pp} - G_{qq}) & \sin^2\theta\, G_{pp} + \cos^2\theta\, G_{qq} \end{bmatrix} \quad (12)
$$

Thus, the diagonal and off-diagonal components of the xy coordinate system are composed of the diagonal components G_{pp} and G_{qq} in the pq coordinate system. This also allows for the size of each component to be adjusted according to the rotational angle θ. The nominal dynamic stiffness in the cutting process can theoretically be made infinitely large by adjusting the equivalent transfer function Φ in Eq. (8) to zero. The diagonal angle components of the transfer function ${}^{pq}\boldsymbol{G}(s)$ in the pq coordinate system need to have a mutually similar relationship, and an appropriate similarity ratio in the two components needs to be set to

achieve this infinitely large value. The similarity mentioned here refers to the conditions in which each component of the frequency response function for an arbitrary frequency has a fixed ratio. Here, the ratio of G_{xx} and G_{xy} is expressed by Eq. (13), using the force ratio K_r and chip flow angle η.

$$\frac{G_{xy}(i\omega_c)}{G_{xx}(i\omega_c)} = -K_r \cos\eta \qquad (13)$$

First, the results based on Eq. (12) of the rotational angle dependencies of the frequency response function in the xy coordinate system are shown in Fig. 4. This figure also includes the equivalent transfer function determined using Eq. (8). Here, $k_p = 2k_q = 2 \times 10^7$ N/m, $\omega_p = \omega_q = 2\pi \times 10^3$ rad/s, $\zeta_p = \zeta_q = 0.03$, $K_r = 0.6$, and $\cos\eta$ =0.6. In other words, the natural frequency and damping ratio in the modal coordinate system are equivalent, and the compliance ratio $|G_{qq}|/|G_{pp}|$ is set to 2. $G_{xx} = G_{pp}$ and $G_{yy} = G_{qq}$ when the rotational angle $\theta = 0°$. The compliance of each component can be seen to vary according to the rotational angle θ. The equivalent transfer function Φ also greatly varied as a result, and a rotational angle-dependent sweet spot was observed where the resonance peak decreased.

Here, the effect of various parameters was analyzed by assuming their values to calculate the equivalent transfer function $\Phi(i\omega_c)$ and determine the effects of decreasing compliance. Fig. 5 shows the results of the influences of the rotational angle θ and $\cos\eta$ on the equivalent transfer function when the compliance ratio $|G_{qq}|/|G_{pp}|$ was set as 2. Here, the maximum negative real part $\max(-\Phi_{re}(i\omega_c))$ of the equivalent transfer function was assessed as an indicator of the chatter stability. The stability limit of chatter vibration is directly dependent on the maximum negative real part, and the system is more stabilized as the maximum negative real part becomes smaller [1]. In other words, the maximum negative real part expresses the effective compliance of the system. K_r is the coefficient that depends on tool–workpiece friction characteristics and the rake angle of the tool; this was set as $K_r = 0.6$ because it often has an empirical value of 0.2–1.0. The maximum negative real part considerably changed with changes in the rotational angle θ and $\cos\eta$ of the coordinate system. The maximum negative real part in particular approached zero across a wide range near $\cos\eta = 0.6$ and rotational angle $\theta = 148°$, resulting in stabilization. Although it depends on the machining conditions, the chip flow angle ranged between $0 \leq \cos\eta \leq 1$. The proposed methods may improve the stability for these reasons, and the optimal rotational angle θ can be seen to be approximately $148°$. In contrast, this may have the opposite intended effect if

the conditions were inappropriate.

Next, Fig. 6 shows the assessment results of the influence of the compliance ratio $|G_{qq}|/|G_{pp}|$ when the rotational angle θ was fixed at $148°$ and K_r was assumed to be 0.6. The figure indicates that for $\cos\eta$, the maximum negative real part became zero in the range where the compliance ratio $|G_{qq}|/|G_{pp}|$ was between 1 and 3. The conditions that satisfy this can be expressed using Eq. (12) and (13).

$$\frac{|G_{qq}|}{|G_{pp}|} = -\frac{K_r \cos\eta \cos^2\theta - \sin\theta\cos\theta}{K_r \cos\eta \sin^2\theta + \sin\theta\cos\theta} \qquad (14)$$

The chip flow angle η varied according to the tool shape and cutting conditions. For example, the flow chip angle η approached $0°$ when the nose radius was large and the radial depth of cut was small, whereas η approached $90°$ for the opposite conditions. In other words, this is a parameter that can be adjusted by the operator at will. Therefore, the chip flow angle η should be selected so that the stability improves with regard to the compliance ratio of the structure. Furthermore, $\cos\eta$ had a value of approximately 1 when the radial depth of cut was small (e.g., during finishing operations), so the compliance ratio $|G_{qq}|/|G_{pp}|$ should be set to a value of approximately 2.5–3.

Next, the influence of the natural frequency error is considered. Errors in natural frequency are generated because of factors like dimensional errors when actually constructing a tool. A robust design for frequency errors is thus required. Figure 7 shows the assessment results of the influence of the natural frequency difference $f_{nq} - f_{np}$ in the pq coordinate system when the rotational angle θ was $148°$ and the compliance ratio $\max(|G_{qq}|) / \max(|G_{pp}|)$ was fixed at 2. The figure shows that the maximum negative real part decreased the most when the natural frequency difference was 0 Hz. This effect was particularly high at approximately $\cos\eta = 0.6$; furthermore, the natural frequency difference had a minimal effect. The maximum negative real part non-symmetrically varied with the frequency error, and higher stability was obtained when f_{np} was higher than f_{nq}.The frequency response functions were compared when the natural frequency difference was set at $f_{nq} - f_{np} = \pm 20\text{Hz}$ to elucidate the causes of this non-symmetry. Figure 8 shows changes in the absolute values of G_{pp} and G_{qq} as well as the real parts of G_{xx}, G_{xy}, and Φ. The figure indicates that profiles of the frequency response functions changed depending on the natural frequency error and were significantly different near the natural frequencies of $real(G_{xx})$ and $real(G_{xy})$. Changes in $real(\Phi)$ were also generated as a result. The change in the frequency f_c that satisfies the

condition $f_{np} \leq f_c \leq f_{nq}$ protruded in particular and became large. The magnitude of the correlation between f_{np} and f_{nq} inverted the direction of change in $real(\Phi)$; thus, the maximum negative real part rapidly changed when $f_{np} \leq f_{nq}$ and the system stiffness with respect to chatter vibration decreased. Meanwhile, the rapid fluctuations in the maximum negative real part did not influence the maximum negative real part when $f_{np} \geq f_{nq}$. Thus, a holder should be fabricated such that f_{np} is slightly larger than f_{nq}. However, the natural frequency difference had to be below the half width (60 Hz in this case) at the very least.

Next, Fig. 9 shows the assessment results of the influence of the chip flow angle η and the force ratio K_r on the maximum negative real part when the rotational angle θ was fixed at 148°, the compliance ratio $|G_{qq}|/|G_{pp}|$ was set at 2, and the natural frequency difference $f_{nq} - f_{np}$ was set at zero. Results showed that there was a chip flow angle η where the maximum negative real part became zero in the range where the force ratio was above 0.35. This relationship can be expressed using the following equation:

$$K_r \cos\eta = \frac{\sin\theta\cos\theta\left(1 - \frac{|G_{qq}|}{|G_{pp}|}\right)}{\frac{|G_{qq}|}{|G_{pp}|}\sin^2\theta + \cos^2\theta} \qquad (15)$$

The stabilization was obtained under conditions of a shallow radial cutting depth, where the chip flow angle η is small when the force ratio K_r is small. Meanwhile, a larger force ratio K_r results in stabilization, where the chip flow angle η is larger; thus, the depth of cut d_r was also thought to increase. Thus, the cutting conditions or compliance ratio $|G_{qq}|/|G_{pp}|$ should be set according to the force ratio of the process.

Next, Fig. 10 shows the assessment results of the influence of the error from the damping ratio fraction ζ_q/ζ_p when the rotational angle θ was fixed at 148°, the maximum compliance ratio $|G_{qq}|/|G_{pp}|$ was set at 2, and the natural frequency difference $f_{nq} - f_{np}$ was set at zero. First, the frequency response functions were observed to be completely similar when the fraction ζ_q/ζ_p was equal to 1, but the half widths no longer matched when the fraction was different, which resulted in deteriorated similarity of the frequency response functions G_{pp} and G_{qq} near the resonanct frequency. Therefore, as seen in the figure, the maximum negative real part was zero and the largest increases in stability were observed when $\cos\eta = 0.6$ and $\zeta_q/\zeta_p = 1$. Meanwhile, the maximum negative real part no longer became zero when ζ_q/ζ_p deviated from 1, and the stiffness against chatter vibration decreased. However, there were no significant

differences in the maximum negative real part when ζ_q/ζ_p =0.5 and ζ_q/ζ_p =2.0; thus, no obvious directionality dependencies were observed with respect to the effect on stability.

As stated above, comparatively robust effects can be achieved by fixing the rotational angle to 148° and appropriately setting up the compliance ratio $|G_{qq}|/|G_{pp}|$ according to the force ratio K_r and the chip flow angle η in the actual cutting process. Furthermore, the similarity of the diagonal components in the pq coordinate system is important, and both the natural frequency difference $f_{np} - f_{nq}$ and damping ratio difference ζ_q/ζ_p can significantly deteriorate performance. However, the influence of the differences can be minimized when $f_{np} - f_{nq} \leq 0$.

4. Proposal of a tool design method using FEM and analysis examples (L/D4 and L/D10)

Section 3 explained how the compliance ratio and similarity between eigen modes were important requirements for ideal anisotropic transfer characteristics to achieve infinitely large dynamic stiffness. This section explains the design method of a structural body which satisfies the requirements for transfer characteristics. An analytical FEM-based approach is used here.

4.1 Design overview of boring tool

Figure 11 shows an overview of the design method for a basic boring tool. An insert tool was attached at the end of the cylindrical boring bar, and the other side of the boring tool was fixed on the fixture base. The structure was axisymmetric if it was a cylindrical bar. Thus, the dynamic characteristics in the radial direction would be isotropic. In this study, anisotropic dynamic stiffness was designed using the mode expansion effects due to the horn shape. As shown in the figure, designing the tapered horn on the free end of the cylindrical bar reduced the stiffness and increased the vibration amplitude in the direction of the thin wall (q direction). Meanwhile, the effect of the vibration amplitude expansion was minimal in the direction of the thick wall (p-direction). This could be used to adjust the compliance ratio between modes. Simultaneously, the horn structure increased the natural frequency by decreasing the inertia on the free-end side. This increased the natural frequency in the high-stiffness p-direction relative to that in the q direction, which created a natural frequency difference. Meanwhile, the natural frequencies between modes had to be matched to improve similarity. Thus, a small notch was made in the p-direction near the base of the boring tool to compensate for this frequency difference. The reduced stiffness caused by this notch was used to

conduct micro-adjustments so that the natural frequencies matched.

The shape was designed using general-use FEM analysis software (ANSYS^{TM}) based on the design principles discussed till now. Here, the L/D ratio, which is the ratio between the protruding length and diameter of the holder, was set to 4 and 10. The designed models are shown in Fig. 12. A boring tool with $\phi 25$ and a length of 100 mm (L/D4) and 250 mm (L/D10) was used as the shape. First, modal analysis was performed to investigate the geometry where the natural frequency difference $\omega_{nq} - \omega_{np}$ in the pq coordinate system became zero. Next, the frequency response function (FRF) was estimated using frequency response analysis, and both the compliance ratio and similarity were confirmed. Rayleigh damping was assumed here, and the coefficients were adjusted to ensure the quality factor Q would be approximately 50. Note that care must be taken because this damping is an empirically estimated value, and there is no assurance that this corresponds with the actual characteristics. Furthermore, a general-use boring tool that simulated a commercially available product was modeled as an isotropic tool in L/D4 for comparison to determine the influence of the fixed portions of the tool on the vibration mode. For L/D10, a two-bladed general-use boring tool which simulated commercially available products with the same L/D was modeled. FRF analysis was then performed for each holder. The quality factor Q, natural frequency f_{np} in the p-direction, maximum compliance $\max(|G_{pp}|)$ in the p-direction, natural frequency difference $f_{nq} - f_{np}$ in the pq-direction mode, and the maximum compliance ratio $\max(|G_{qq}|) / \max(|G_{pp}|)$ in each model were determined. Dimensions and design values used in analysis as well as the analysis results are summarized in Table 1. Details of the design are shown below.

4.2 Design of L/D4 boring tool

The desired vibration mode cannot be obtained when the tool end where the insert tool is attached has an asymmetric shape and the balance between inertia and stiffness is disrupted. Therefore, a dummy insert tool was attached at the opposite end of the insert at the end, as shown in Fig. 12. The tool was designed to ensure a symmetric structure. However, general-use L/D4 tools without any notch or horn shape were modeled as commercially available general-use holders. Therefore, the dummy insert was not attached here. FRF estimation results of the general-use tool and the L/D4 tool designed using the proposed method are shown in Fig. 13. Model (I4) was the general-use tool (isotropic), and model (A4) was the proposed boring tool. Each directional component of the FRF and the frequency where the compliance is maximal, i.e.,

damped natural frequency, are shown. The general-use tool (I4) had a compliance ratio $\max(|G_{yy}|) / \max(|G_{xx}|)$ of 0.93 and was roughly isotropic. Furthermore, a slightly asymmetric component was fabricated. This is thought to be because the overall structure including the jig is not a completely axisymmetric structure. The off-diagonal component G_{xy} of the general-use tool had a similar shape to the diagonal component G_{xx}, and the phase was not inverted. Therefore, the off-diagonal component G_{xy} was predicted to influence the direction which increases the equivalent transfer function $\Phi = \cos\eta\, G_{xx} + G_{xy}/K_r$. In other words, anisotropy is thought to function in a manner that destabilizes the system.

Meanwhile, the compliance ratio $\max(|G_{qq}|) / \max(|G_{pp}|)$ of the proposed tool (A4) was approximately 1.37 in the pq coordinate system and was anisotropic. Simultaneously, roughly similar characteristics were obtained. The natural frequency difference was $f_{nq} - f_{np} = 1809.8 - 1813.2 = -3.4$ Hz and was sufficiently smaller than the half width (35 Hz); the natural frequency in the p-direction was high. However, the off-diagonal components G_{pq} and G_{qp} were not small, with values of 2.5 μm/N. The compliance ratio of the off-diagonal component G_{xy} and diagonal component G_{xx} was approximately 0.13 in the xy coordinate system. Furthermore, the diagonal component and off-diagonal component were roughly similar, and their phases were inverted. Therefore, G_{xx} and G_{xy} were predicted to cancel out each other and minimize the equivalent transfer function Φ when $K_r \cos\eta$ was 0.13. This agrees with the relationship between the compliance ratio $\max(|G_{qq}|) / \max(|G_{pp}|)$ and $K_r \cos\eta$ in the analysis results shown in Fig. 6.

Figure 14 shows as an example of a vector diagram of the equivalent transfer function $\Phi(i\omega_c)$ as well as the diagonal component G_{xx} and off-diagonal component G_{xy} of the FRFs determined by setting $K_r = 0.6$ and $\cos\eta = 0.22$. Compared with the general-use tool (I4), the proposed tool (A4) had a somewhat larger diagonal angle element G_{xx} of the FRF because of the tapered horn and notch. Meanwhile, the proposed boring tool was smaller for the equivalent transfer function $\Phi(i\omega_c)$. Comparisons of the maximum negative real part showed that the proposed tool could be estimated to be more stable than the general-use tool by a factor of approximately 1.7. In other words, the nominal tool stiffness somewhat increased due to the proposed design. However, the improved stability effects against chatter vibration could be obtained by suitably selecting combinations of the force ratio and the chip flow angle.

Next, Fig. 15 shows the analysis results of the influence of the force ratio K_r and chip flow rate η on

the maximum negative real part $\max\left(-\Phi_{re}(i\omega_c)\right)$ of the FRF. The boundary line where the maximum negative real part $\max\left(-\Phi_{re}(i\omega_c)\right)$ is 1 μm/N is shown in the figure. It can be seen that the maximum negative real part $\max\left(-\Phi_{re}(i\omega_c)\right)$ decreased and the nominal stiffness was improved for the general-use tool (I4) when the chip flow angle η and force ratio K_r were large. The minimal maximum negative real part $\min\left(\max\left(-\Phi_{re}(i\omega_c)\right)\right) = 0.26$ μm/N was obtained when $(K_r, \eta) = (1, 89°)$ under the analyzed range. The value of $\cos\eta$ also became small when the chip flow angle η was large, and the influence of the diagonal component G_{xx} also decreased. Furthermore, the influence of the off-diagonal component G_{xy} decreased when the force ratio K_r was large. Therefore, the process stability tended to be improved under conditions where the chip flow angle η and force ratio K_r were large. Meanwhile, the chip flow angle η could not be increased under the finishing cutting conditions, where the nose radius was large and the radial depth of cut was small. Therefore, stabilization may only be possible under limited conditions such as rough processing.

A minimum value of the maximum negative real part $\min\left(\max\left(-\Phi_{re}(i\omega_c)\right)\right) = 0.33$ μm/N was obtained for the proposed boring tool (A4) under the conditions $(K_r, \eta) = (1, 81.7°)$. This minimum value was slightly larger than that in the general-use tool; however, the range under which the maximum negative real part decreased was slightly different from the general-use tool. The range in which the maximum negative real part decreased was widely distributed relative to the general-use tool. Similar to that of the general-use tool, stabilization was more likely to occur under conditions where the chip flow angle η and force ratio K_r were large. On the other hand, the stability also effectively increased at approximately $K_r \cos\eta = 0.13$. Therefore, stabilization may be achieved with conditions ranging from a large to small chip flow angle η, depending on the combinations with the force ratio K_r. Unlike the general-use tool, the decreased maximum negative real part under conditions where the chip flow angle η was small suggests that stabilization could be achieved even under finishing cutting conditions. In other words, stability may possibly be improved from rough cutting to finishing cutting using the proposed boring tool.

4.3 Design of L/D10 boring tool

Next, the L/D10 tool design was analyzed. The five design types shown in Table 1 were compared. Model (I10) was an isometric general-use design. Models (A10-1)–(A10-4) were designed using the proposed

method. The proposed tools (A10-1) and (A10-2) were designed to have a compliance ratio of 1.67 and 1.46, respectively, for the diagonal component in the pq coordinate system. The proposed tool (A10-3) was designed so that the natural frequency in the p-direction was larger by approximately 50 Hz, and the influence of frequency error was assessed. The proposed tool (A10-4) had the same shape as that of the (A10-1) tool, but was designed using FEM analysis to have a quality factor Q approximately three times higher at approximately 150, and the influence of the quality factor Q was assessed.

First, comparisons of the FRFs (G_{xx} and G_{xy}) for each condition are shown in Fig. 16. The compliance significantly increased and the natural frequency decreased when compared to the results of the L/D4 design. The general-use tool (I10) was isotropic; thus, the off-diagonal component G_{xy} was relatively small. The diagonal component G_{xx} and off-diagonal component G_{xy} in the proposed tools (A10-1) and (A10-2) had a mostly similar shape, and the fact that they had offset one another may have resulted in the increased stiffness of the equivalent transfer function. Meanwhile, changes in the mode ratio in the proposed tool (A10-3) depended on the frequency due to natural frequency differences; it can be seen that the diagonal component G_{xx} and off-diagonal component G_{xy} did not have a similar shape. Similar to (A10-1), the proposed tool (A10-4) had similar shapes of the diagonal angle element G_{xx} and off-diagonal component G_{xy}, but G_{xx} and G_{xy} increased by a factor of four with the increased Q value.

Next, Fig. 17 shows the analysis results of the influence of force ratio K_r and chip flow angle η with respect to the maximum negative real part $\max\left(-\Phi_{re}(i\omega_c)\right)$ of the equivalent transfer function. Like the L/D4 results, the general-use tool (I10) had a decreased maximum negative real part $\max\left(-\Phi_{re}(i\omega_c)\right)$ and showed improved stability under conditions where the chip flow angle η and force ratio K_r were large. A minimal value of the maximum negative real part $\min\left(\max\left(-\Phi_{re}(i\omega_c)\right)\right)$ =1.73 μm/N was achieved under the condition of $(K_r, \eta) = (1, 89°)$. The boundaries where the maximum negative real part $\max\left(-\Phi_{re}(i\omega_c)\right)$ was equal to 1.73 μm/N in the proposed tool models (A10-1)–(A10-4) are shown as white lines in the figures. In other words, the domain inside the white line can exceed the highest stability obtained with the general-use tools. The compliance of the equivalent transfer function decreased near the conditions where $K_r \cos\eta$ =0.25 for the proposed method, and the effects of the improved stability were confirmed. The minimal value of the maximum negative real part $\min\left(\max\left(-\Phi_{re}(i\omega_c)\right)\right)$ was approximately 0.13 μm/N for the proposed tool (A10-1), and a stability improvement by a factor of

approximately 13 relative to the general-use tool was achieved. The L/D10 was expected to exhibit stability improvement equivalent to or higher than that of L/D4 under the most improved conditions. Thus, stability could be further improved with this method by selecting the suitable combinations of the compliance ratio $\max(|G_{qq}|) / \max(|G_{pp}|)$, force ratio K_r, and chip flow angle η. Stability was improved even under conditions where the chip flow angle η was small; thus, the L/D10 is thought to be effective for finishing cutting similar to L/D4.

Comparisons of the proposed tools (A10-1) and (A10-2) showed that the tools had similar tendencies, but the proposed tool (A10-2) had a higher value for the minimal of maximum negative real part $\min(\max(-\Phi_{re}(i\omega_c)))$ and a lower stability. This was thought to depend on the similarity in the shapes of the FRF components G_{xx} and G_{xy}. Figure 18 shows the real parts of the components of the FRF G_{xx} and G_{xy} for the proposed tools (A10-1) and (A10-2). The figure indicates that the natural frequency at which the real part is zero in the proposed tool (A10-1) corresponded well with G_{xx} and G_{xy}. Meanwhile, a slight difference was observed in the proposed tool (A10-2). As shown in Table 1, the natural frequency difference $f_{nq} - f_{np}$ between modes was low at -0.4 Hz; however, it can be seen that the minimal of the maximum negative real part $\min(\max(-\Phi_{re}(i\omega_c)))$ was highly sensitive to change. The stability in the proposed tool (A10-3) conversely decreased more than the general-use tool because the natural frequency difference was significant. Compared with that of the proposed tool (A10-1), the stability of (A10-4) decreased by approximately 1/6, and reductions were observed in the stable range where the maximum negative real part $\max(-\Phi_{re}(i\omega_c))$ was below 1.73 μm/N. This was because the similarity of G_{xx} and G_{xy} decreased due to the system developing low damping characteristics. Roughly identical phenomena were confirmed after assessing the influence of the Q value under various conditions. These results show that designing the system so that the Q value is smaller in practical applications is extremely important.

The above investigation indicates that sufficient effects may occur even with L/D10 if the transfer characteristics satisfy the desired compliance ratio and mode similarity. A suitable tool shape and processing conditions need to be selected to achieve the desired force ratio and chip flow angle as well as stability. Furthermore, minimizing the natural frequency error is necessary, and system damping should be designed to be large.

5. Conclusions

A novel boring tool design method that suppresses the chatter vibration is proposed here. The proposed method uses anisotropy of the boring tool to make the dynamic stiffness in the cutting process infinitely large. The stability of the process may be achieved by simply designing the tool shape in an optimal manner. Our study explained basic design methods and analytically clarified the effects of design errors on nominal dynamic stiffness. The obtained conclusions are summarized below. Results of the assessment of characteristics of the designed tool and stability limit analysis as well as the verification of the processing experiments are discussed in further detail in Part 2.

1. A system where the natural frequencies in the modal coordinate system (pq coordinate system) match ($\omega_{np} = \omega_{nq}$) and where the compliance ratio is larger than 1 ($|G_{qq}|/|G_{pp}| > 1$) was designed using the proposed method. Furthermore, the desired anisotropic transfer characteristics that robustly improve the nominal dynamic stiffness against changes in the chip flow angle could be obtained by setting the rotational angle of the modal coordinate system for the process coordinate system to 148°.
2. The range of optimal compliance ratio was set to $1 < |G_{qq}|/|G_{pp}| < 3$ when the FRF in the modal coordinate system satisfied similarity. The compliance ratio also had to be optimally designed according to the force ratio and the desired chip flow angle of the subject cutting process.
3. The similarity of the diagonal components for the FRF in the pq coordinate system was important. The natural frequency and damping ratio had to be adjusted so that they matched between modes to improve similarity. However, the influence of errors could be minimized when the natural frequency difference was $f_{nq} - f_{np} \leq 0$.
4. A method that matchs the natural frequencies and designs a two-degree-of-freedom system with a desired compliance ratio was proposed by setting up a tapered horn shape at the free-end side of the boring tool and adding notches at the base of the held side. A dimension design method for achieving the desired vibration characteristics was proposed using FEM analysis.
5. Stability was confirmed to dramatically increase under conditions where the desired combination of the force ratio K_r and chip flow angle η were satisfied in the proposed tool after analyzing the FRFs determined through FEM analysis. Effects that further improve the stability from the rough

cutting step to finishing cutting step can be expected using the proposed tool.

Acknowledgments

The Authors thank Mr. Nishimura and Mr. Watanabe. They made enormous contributions in the early stages of research.

Funding sources

This work was partially supported by JSPS KAKENHI Grant Number 22760097.

References

[1] Altintas Y. Manufacturing automation 2nd edition, Cambridge University Press, 2012.

[2] Zeng S, Wan X, Li W, Yin Z, Xion S. A Novel Approach to Fixture Design on Suppressing Machining Vibration of Flexible Workpiece. Int J Mach Tools Manuf 2012;58:29–43.

[3] Thorenz B, Friedrich M, Westermann H H, Döpper F. Evaluation of the influence of different inner cores on the dynamic behavior of boring bars. Procedia CIRP 2019;81:1171–6.

[4] Zhang Y, Ren Y, Tian J, Ma J. Chatter stability of the constrained layer damping composite boring bar in cutting process. J Vib Control 2019;25(16):2204–14.

[5] Ghorbani S, Polushin NI. Effect of Composite Material on Damping Capacity Improvement of Cutting Tool in Machining Operation Using Taguchi Approach. World Academy of Science, Engineering and Technology International Journal of Chemical, Molecular, Nuclear, Materials and Metallurgical Engineering 2015;9(12):1222–32.

[6] Denkena B, Bergmann B, Teige C. Frictionally damped tool holder for long projection cutting tools. Prod Eng 2018;12:715–22.

[7] Paul PS, Raja P, Aruldhas P, Pringle S, Shaji E. Effectiveness of particle and mass impact damping on tool vibration during hard turning process. J Eng Manuf 2018;232(5):776–86.

[8] Onozuka H, Utsumi K, Kato T, Takahashi H, Obikawa T. Optimal Design of a Damped Arbor for Heavy-Duty Machining of Giant Parts. J Adv Mech Des Syst Manuf 2013:7(2);171–86.

[9] Slocum AH, Marsh ER, Smith DH. A new damper design for machine tool structures: the replicated internal viscous damper. Precis Eng 1994;16(3):174–83.

[10] Rivin EI, Kang HL, KopsL. Improving dynamic performance of cantilever boring bars. CIRP Annals 1989;38(1):377–80.

[11] Liu PX, Jiang B, Wu X, Yue C. Study on Dynamic Properties of Damping Boring Bar with Large Ratio of Length to Diameter. Mater Sci Forum 2014;800(801):489–94.

[12] Lee EC, Nian CY, Tarng YS. Design of a dynamic vibration absorber against vibrations in turning operations. J Mater Proces Technol 2001;108(3):278–85.

[13] Yoshimura M. Vibration-Proof Design of Boring Bar With Multidegree-of-Freedom Dampers. J Mech Des 1986;108(4):442–7.

[14] Hayati S, Hajaliakbari M, Rajabi Y, Rasaee S. Chatter reduction in slender boring bar via a tunable holder with variable mass and stiffness. Proc Inst Mech Eng B 2018;232(12):2098–108.

[15] Matsubara A, Maeda M, Yamaji I. Vibration suppression of boring bar by piezoelectric actuators and LR circuit. CIRP Annals 2014;63(1):373–6.

[16] Chen F, Lu X, Altintas Y. A novel magnetic actuator design for active damping of machining tools. Int J Mach Tools Manuf 2014;85:58–69.

[17] Wang M, Fei R. On-Line Chatter Detection & Control in Boring Based on an Electrorheological Fluid. Mechatronics 2001;11(7):779–92.

[18] Fallah M, Moetakef-Imani B. Adaptive inverse control of chatter vibrations in internal turning operations. Mech Syst Signal Proces 2019;129(15):91–111.

[19] Suzuki N, Nishimura K, Shamoto E, Yoshino K. Effect of cross transfer function on chatter stability in plunge cutting. J Adv Mech Des Sys Manuf 2010;4(5):883–91.

[20] Suzuki N, Nishimura K, Watanabe R, Kato T, Shamoto E. Development of novel anisotropic boring tool for chatter suppression. Procedia CIRP 2012;1:56–9.

[21] Takahashi W, Suzuki N, Shamoto E, Design of Anisotropic Boring Tools With L/D = 10 for Chatter Free Cutting. MSEC 2017;2928(V003T04A055);5.

[22] Colwell L. Predicting the angle of chip flow for single-point cutting tools. Trans ASME 1954;76:199.

Figure captions:

Fig. 1 Schematic illustration of the boring process with chatter vibration.

Fig. 2 Block diagram of the boring process with chatter vibration.

Fig. 3 Relative relationship between the xy coordinate system and the pq coordinate system.

Fig. 4 Influence of rotational angle θ on compliance components in the xy coordinate system.

Fig. 5 Influence of rotational angle θ and $\cos\eta$ on $\max\left(-\Phi_{real}(i\omega)\right)$. ($k_p = 2k_q = 2\times10^7$ N/m, $\omega_p = \omega_q = 2\pi\times10^3$ rad/s, $\zeta_p = \zeta_q = 0.03$, $K_r = 0.6$)

Fig. 6 Influence of compliance ratio and $\cos\eta$ on $\max\left(-\Phi_{real}(i\omega)\right)$. ($k_p = 2\times10^7$ N/m, $\omega_p = \omega_q = 2\pi\times10^3$ rad/s, $\zeta_p = \zeta_q = 0.03$, $\theta = 148°$, $K_r = 0.6$)

Fig. 7 Influence of frequency difference $f_{nq} - f_{np}$ and $\cos\eta$ on $\max\left(-\Phi_{real}(i\omega)\right)$. ($k_p = 2k_q = 2\times10^7$ N/m, $\omega_p = 2\pi\times10^3$ rad/s, $\zeta_p = \zeta_q = 0.03$, $\theta = 148°$ $K_r = 0.6$)

Fig. 8 Frequency response functions with inconsistent natural frequencies of f_{np} and f_{nq}.

Fig. 9 Influence of force ratio K_r and chip flow angle η on $\max\left(-\Phi_{re}(i\omega)\right)$. ($k_p = 2k_q = 2\times10^7$ N/m, $\omega_p = \omega_q = 2\pi\times10^3$ rad/s, $\zeta_p = \zeta_q = 0.03$, $\theta = 148°$)

Fig. 10 Influence of damping ratio ζ_q/ζ_p and $\cos\eta$ on $\max\left(-\Phi_{re}(i\omega)\right)$.($2|G_{pp}| = |G_{qq}| = 1.067\times10^{-6}$ m/N, $\omega_p = \omega_q = 2\pi\times10^3$ rad/s, $\zeta_p = 0.03$ $\theta = 148°$, $K_r = 0.6$)

Fig. 11 Design method of the bending mode with anisotropy in the orthogonal directions.

Fig. 12 Schematics of the designed isotropic and anisotropic tools.

Fig. 13 FRFs of the L/D4 boring tools in pq and xy coordinate systems estimated by FEM.

Fig. 14 Vector diagrams of the equivalent transfer functions of L/D4 tools with $K_r = 0.6$ and $\cos\eta = 0.22$.

Fig. 15 FRFs of the proposed L/D4 boring tool in the pq and xy coordinate systems.

Fig. 16 Frequency response functions of the designed boring bars. (G_{xx}, G_{xy})

Fig. 17 Minimum real part of the equivalent transfer function.

Fig. 18 Real parts G_{xx} and G_{xy} of FRFs of the designed boring tools (A10-1) and (A10-2).

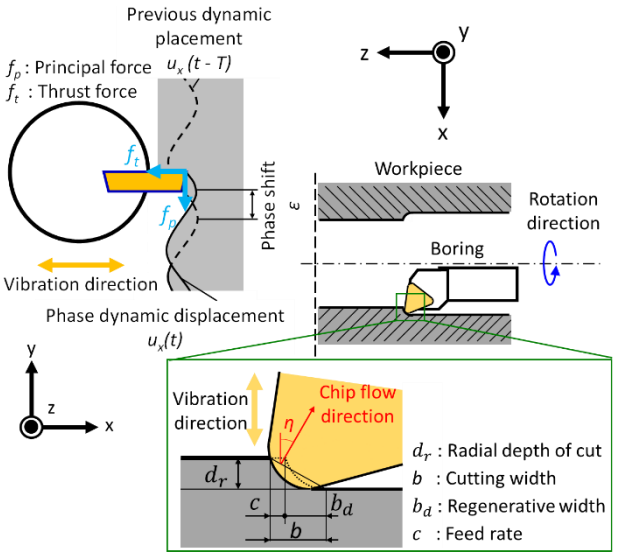

Fig. 1 Schematic illustration of the boring process with chatter vibration.

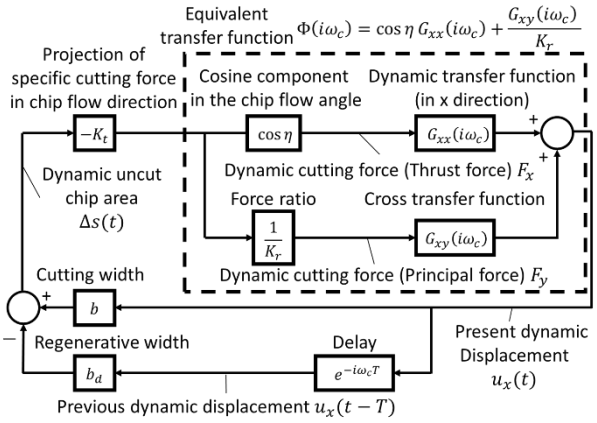

Fig. 2 Block diagram of the boring process with chatter vibration.

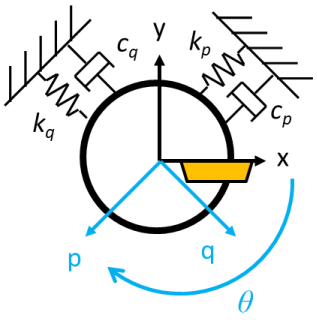

Fig. 3 Relative relationship between the xy coordinate system and the pq coordinate system.

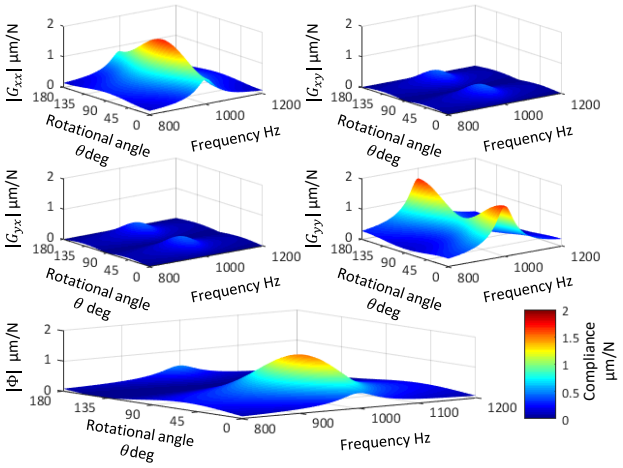

Fig. 4 Influence of rotational angle θ on compliance components in the xy coordinate system.

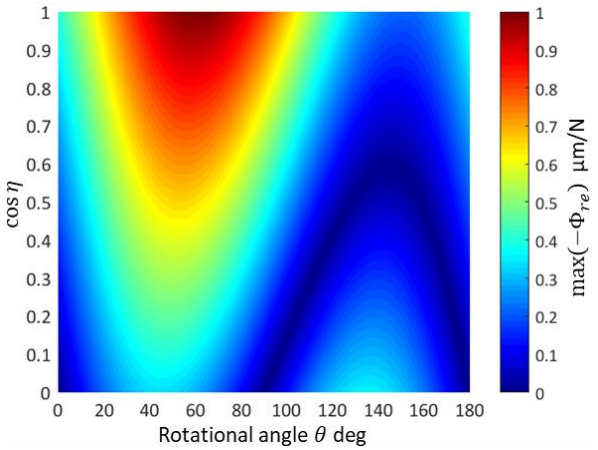

Fig. 5 Influence of rotational angle θ and $\cos\eta$ on $\max\left(-\Phi_{real}(i\omega)\right)$. ($k_p = 2k_q = 2\times10^7$ N/m, $\omega_p = \omega_q = 2\pi\times10^3$ rad/s, $\zeta_p = \zeta_q = 0.03$, $K_r = 0.6$)

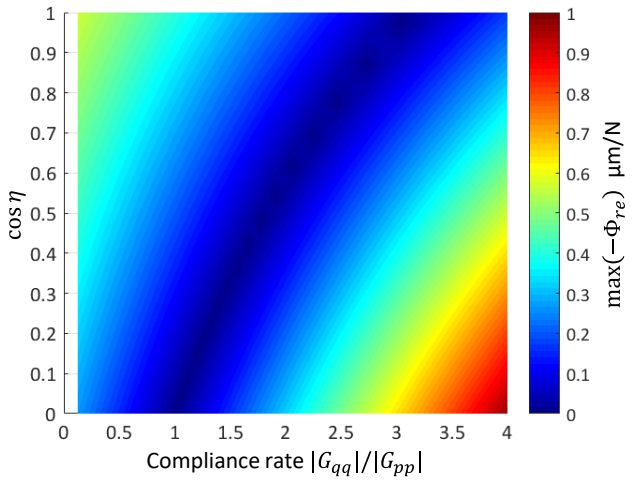

Fig. 6 Influence of compliance ratio and $\cos\eta$ on $\max\left(-\Phi_{real}(i\omega)\right)$. ($k_p = 2 \times 10^7$ N/m, $\omega_p = \omega_q = 2\pi \times 10^3$ rad/s, $\zeta_p = \zeta_q = 0.03$, $\theta = 148°$, $K_r = 0.6$)

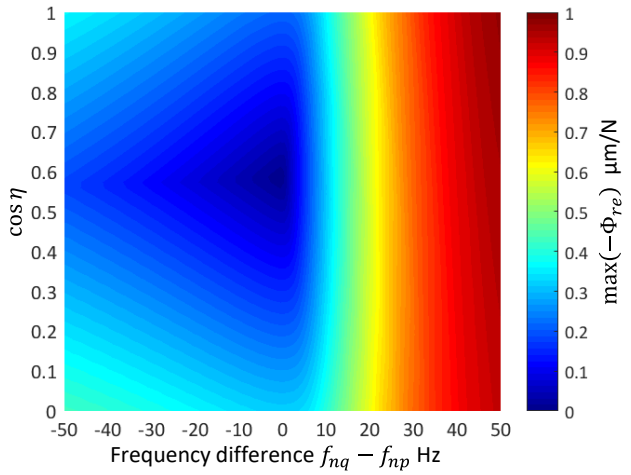

Fig. 7 Influence of frequency difference $f_{nq} - f_{np}$ and $\cos\eta$ on $\max\left(-\Phi_{real}(i\omega)\right)$. ($k_p = 2k_q = 2 \times 10^7$ N/m, $\omega_p = 2\pi \times 10^3$ rad/s, $\zeta_p = \zeta_q = 0.03$, $\theta = 148°$ $K_r = 0.6$)

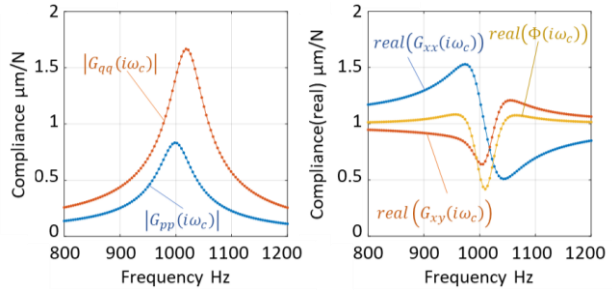

(a) $f_{np} = 1000$ Hz, $f_{nq} = 1020$ Hz

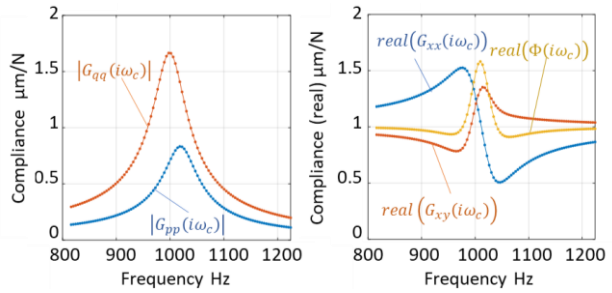

(b) $f_{np} = 1020$ Hz, $f_{nq} = 1000$ Hz

Fig. 8 Frequency response functions with inconsistent natural frequencies of f_{np} and f_{nq}.

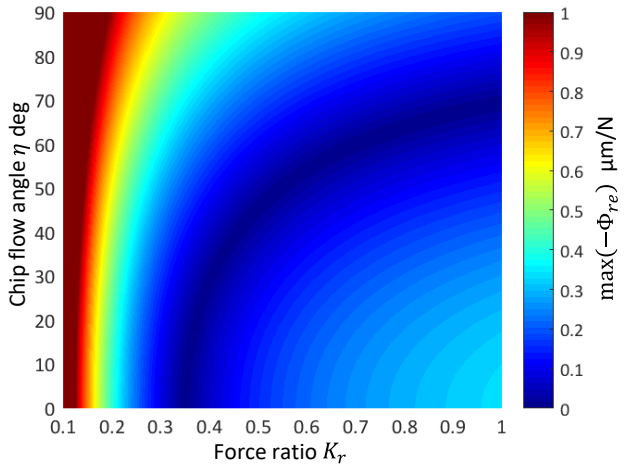

Fig. 9 Influence of force ratio K_r and chip flow angle η on $\max\left(-\Phi_{re}(i\omega)\right)$. ($k_p = 2k_q = 2 \times 10^7$ N/m, $\omega_p = \omega_q = 2\pi \times 10^3$ rad/s, $\zeta_p = \zeta_q = 0.03$, $\theta = 148°$)

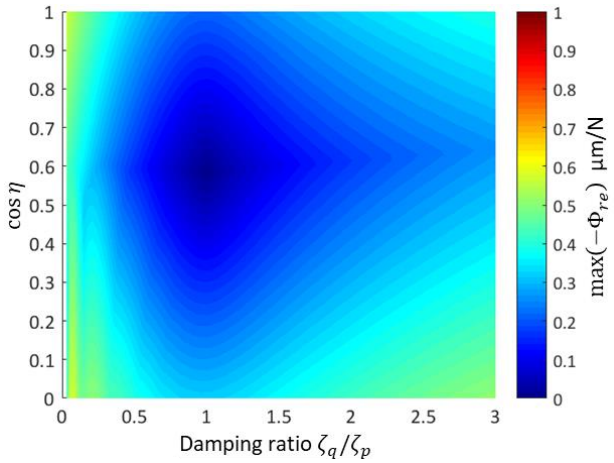

Fig. 10 Influence of damping ratio ζ_q/ζ_p and $\cos\eta$ on $\max(-\Phi_{re}(i\omega))$.($2|G_{pp}| = |G_{qq}| = 1.067 \times 10^{-6}$ m/N, $\omega_p = \omega_q = 2\pi \times 10^3$ rad/s, $\zeta_p = 0.03$ $\theta = 148°$, $K_r = 0.6$)

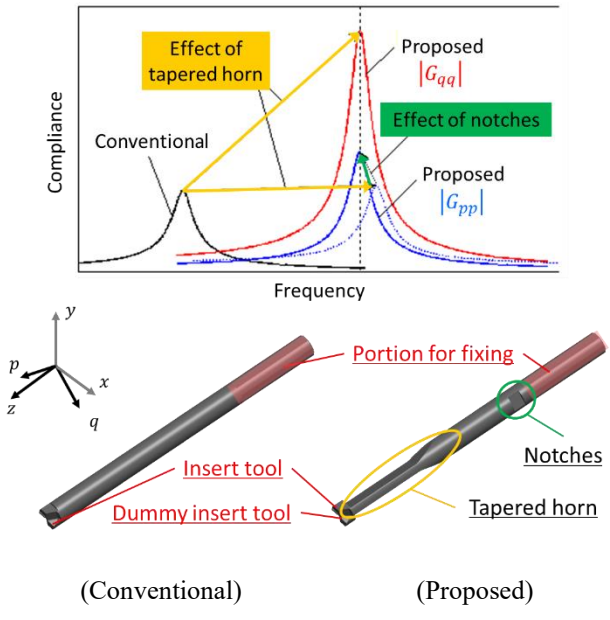

Fig. 11 Design method of the bending mode with anisotropy in the orthogonal directions.

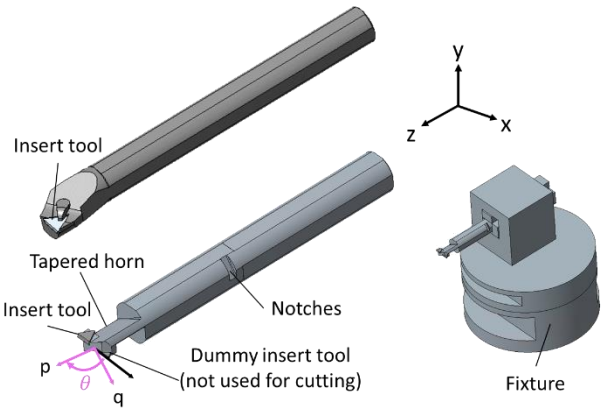

(a) Isotropic and anisotropic boring tool (L/D4)

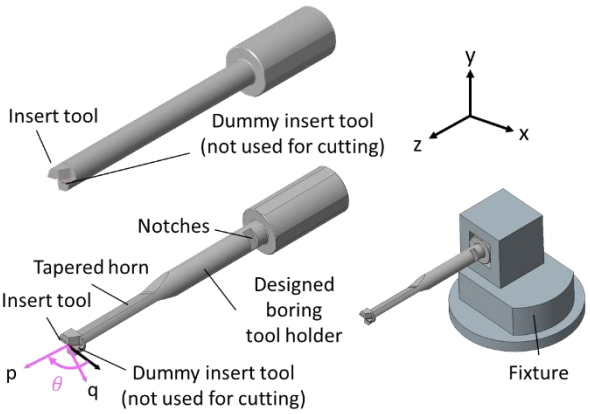

(b) Isotropic and anisotropic boring tool (L/D10)

Fig. 12 Schematics of the designed isotropic and anisotropic tools.

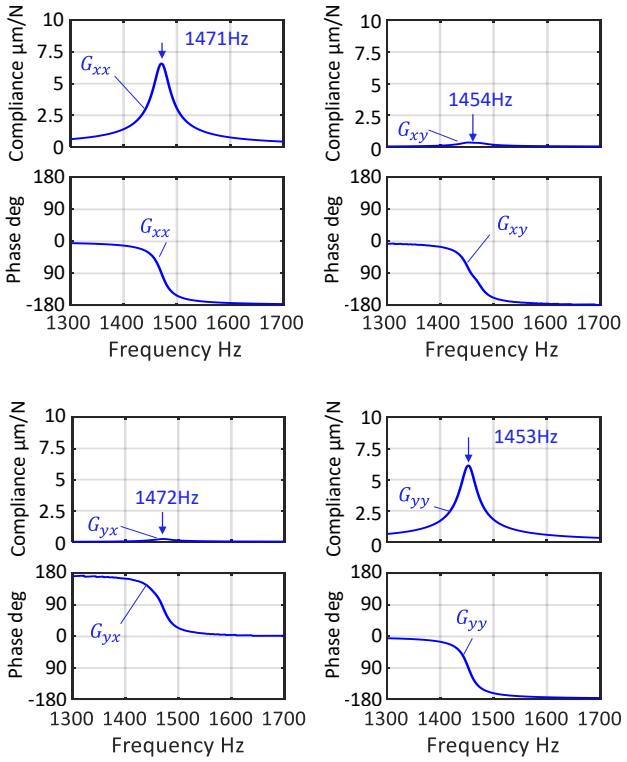

(a) I4 (Conventional)

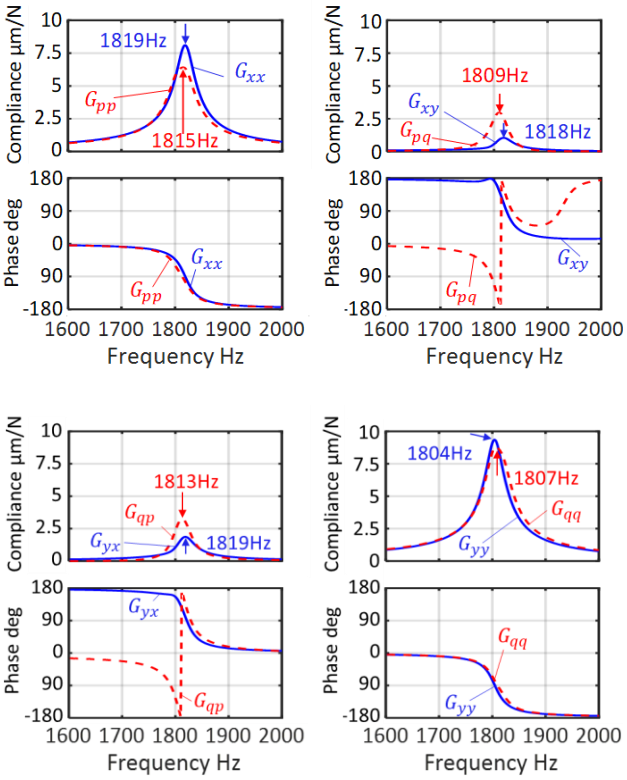

(b) A4 (Proposed)

Fig. 13 FRFs of the L/D4 boring tools in pq and xy coordinate systems estimated by FEM.

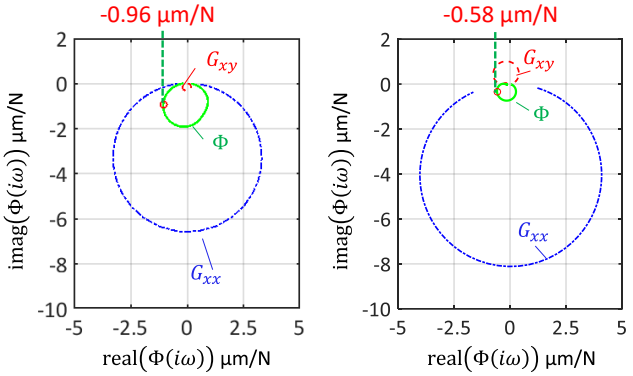

(a) I4 (Conventional) (b) A4 (Proposed)

Fig. 14 Vector diagrams of the equivalent transfer functions of L/D4 tools with $K_r = 0.6$ and $\cos\eta = 0.22$.

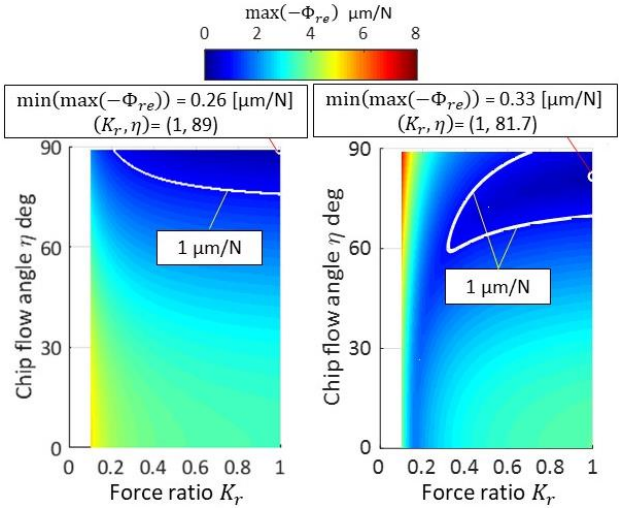

(a) I4 (Conventional) (b) A4 (Proposed)

Fig. 15 FRFs of the proposed L/D4 boring tool in the pq and xy coordinate systems.

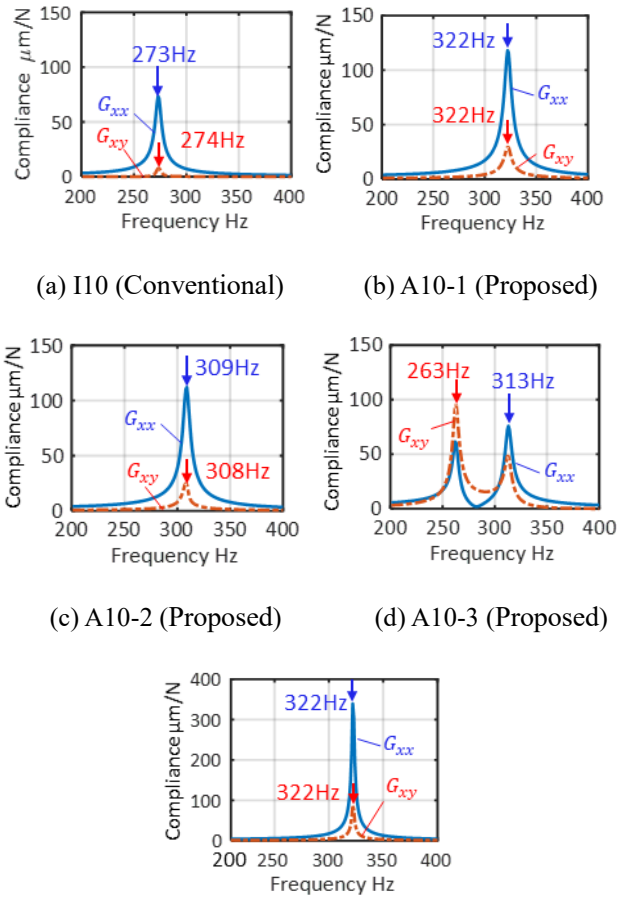

(a) I10 (Conventional) (b) A10-1 (Proposed)

(c) A10-2 (Proposed) (d) A10-3 (Proposed)

(e) A10-4 (Proposed)

Fig. 16 Frequency response functions of the designed boring bars. (G_{xx}, G_{xy})

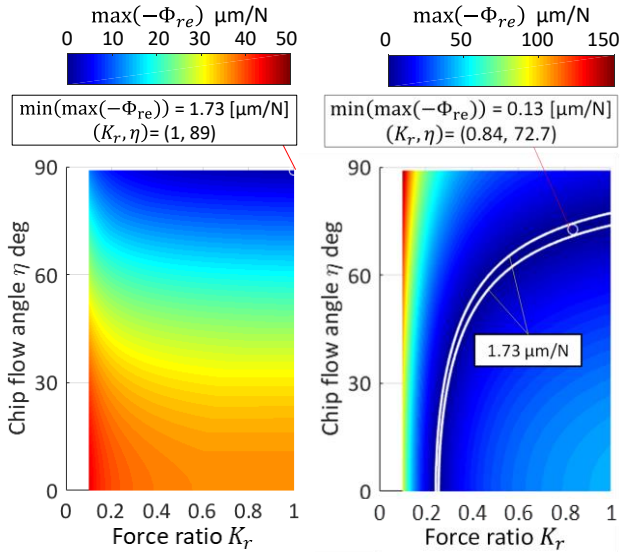

(a) I10 (Conventional) (b) A10-1 (Proposed)

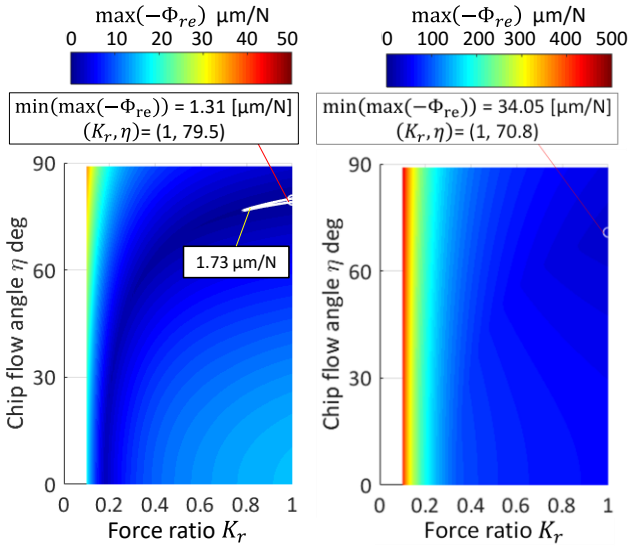

(c) A10-2 (Proposed) (d) A10-3 (Proposed)

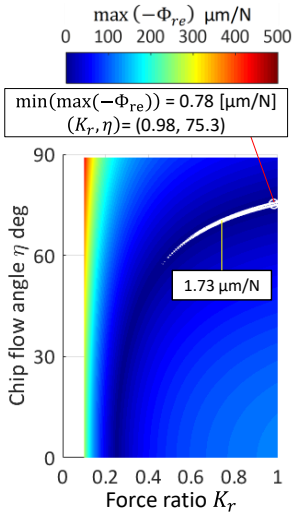

(e) A10-4 (Proposed)

Fig. 17 Minimum real part of the equivalent transfer function.

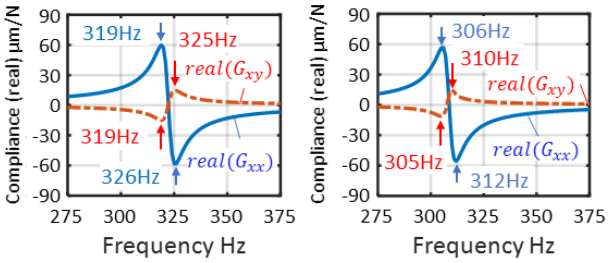

(a) A10-1 (Proposed) (b) A10-2 (Proposed)

Fig. 18 Real parts G_{xx} and G_{xy} of FRFs of the designed boring tools (A10-1) and (A10-2).

Table 1 Dimensions of the designed boring tools and their quality factors, and the performance of each factor.

L/D	Structural dynamics	Model	Notch depth mm	Notch width mm	Horn thickness mm	Horn length mm	Q	Natural frequency in p axis f_{np} Hz	Maximum compliance in p axis $\max(\lvert G_{pp}\rvert)$ μm/N	Natural frequency difference $f_{nq}-f_{np}$ Hz	Compliance ratio $\frac{\max(\lvert G_{qq}\rvert)}{\max(\lvert G_{pp}\rvert)}$
4	Isotropic	I4	0	0	0	0	47	1471	6.6	-18.1	0.93
	Anisotropic	A4	2.6	5	5	28	52	1813	6.4	-3.4	1.37
10	Isotropic	I10	0	0	0	0	47	273	73.4	0.3	1.0
10	Anisotropic	A10-1	5	10	6.8	89	52	323	98.2	0.1	1.67
		A10-2			8.8	107	50	309	98.8	-0.4	1.46
		A10-3			8.8	133	51	313	106.4	-50.4	1.99
		A10-4			6.8	89	146	323	262.2	0.1	1.72